

AperTO - Archivio Istituzionale Open Access dell'Università di Torino

**Visible light responsive heterostructure HTDMA-BiPO<sub>4</sub> modified clays for effective diclofenac sodium oxidation: Role of interface interactions and basal spacing**

**This is the author's manuscript**

*Original Citation:*

*Availability:*

This version is available <http://hdl.handle.net/2318/1885768> since 2025-01-22T10:45:50Z

*Published version:*

DOI:10.1016/j.jwpe.2022.102788

*Terms of use:*

Open Access

Anyone can freely access the full text of works made available as "Open Access". Works made available under a Creative Commons license can be used according to the terms and conditions of said license. Use of all other works requires consent of the right holder (author or publisher) if not exempted from copyright protection by the applicable law.

(Article begins on next page)

1 **Visible light responsive heterostructure HTDMA-BiPO<sub>4</sub> modified clays for**  
2 **effective diclofenac oxidation: role of interface interactions and basal spacing**

3 *Imen Fellah<sup>1</sup>, Ridha Djellabi<sup>2,\*</sup>, Hédi Ben Amor<sup>1</sup>, Nesrine Abderrahim<sup>1</sup>, Claudia L. Bianchi<sup>2</sup>, Alessia*  
4 *Giordana<sup>3</sup>, Giuseppina Cerrato<sup>3</sup>, Noureddine Hamdi<sup>4</sup>*

5 <sup>1</sup>*Engineering school (ENIG), RL Processes, Energetic, Environment and Electric Systems*  
6 *(PEESE) University of Gabes. Gabes 6072, Tunisia.*

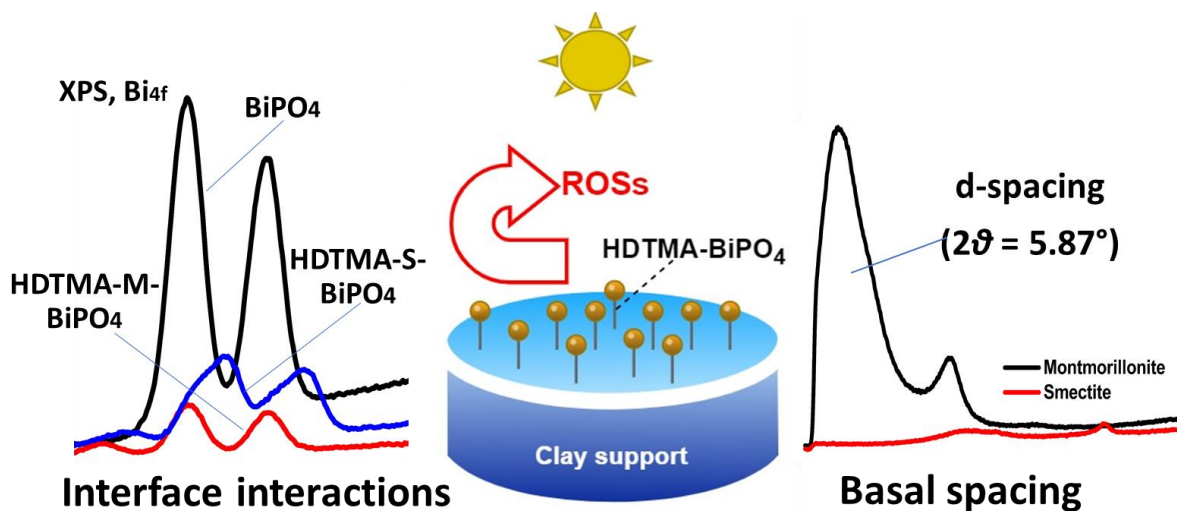
7 <sup>2</sup>*Department of Chemistry, University of Milan, Via Golgi 19, Milano 20133, Italy*

8 <sup>3</sup>*University of Gabès, Higher Institute of Sciences and Techniques of Waters, Tunisia.*

9 <sup>4</sup>*Department of Chemistry, University of Turin, Via Pietro Giuria 7, 10125 Turin, Italy*

10

11 **Graphical abstract**



12

13

14

15

16

17

18

19

20

21 **Abstract,**

22 In the present study, we investigated comparatively the role of hexadecyltrimethylammonium  
23 bromide (HDTMA) in enhancing the adsorption and photocatalytic activity of BiPO<sub>4</sub> coated  
24 Montmorillonite (M-BiPO<sub>4</sub>), and BiPO<sub>4</sub> coated smectite (S-BiPO<sub>4</sub>). Firstly, the direct hybridization  
25 of BiPO<sub>4</sub> with clays results in enhanced adsorption and photocatalytic efficiency for the oxidation of  
26 diclofenac under solar light compared to bare BiPO<sub>4</sub>. Due to the different interlayer spacing of  
27 montmorillonite (big) and smectite (small), the hybridization of both BiPO<sub>4</sub> and HDTMA on the  
28 surface of clays led to different mechanistic pathways. In terms of montmorillonite, the insertion of  
29 BiPO<sub>4</sub> and HDTMA can be realized between the interlayer, while in the case of the smectite, they  
30 might be fixed on the external surface. HDTMA reacts better with BiPO<sub>4</sub> set on the external surface  
31 to form better heterostructure, as proved by XPS analysis. No peak shifting was observed in Bi<sub>4f</sub> high  
32 resolution in HDTMA-M-BiPO<sub>4</sub>, while a strong shift by 1.3 eV along with an obvious change in the  
33 shape of peaks was noticed in HDTMA-S-BiPO<sub>4</sub>. In addition, the P<sub>2p</sub> profiles show a positive peak  
34 shifting by around 0.7 and 3 eV for HDTMA-M-BiPO<sub>4</sub> and HDTMA-S-BiPO<sub>4</sub>, respectively.  
35 Regarding the adsorption and photocatalytic tests, at lower concentration (20 ppm), M-BiPO<sub>4</sub> was  
36 several times more effective than S-BiPO<sub>4</sub>. However, the coating of clays by BiPO<sub>4</sub> and HDTMA  
37 showed a different manner, wherein HDTMA-S-BiPO<sub>4</sub> achieved an oxidation rate of around 88%  
38 under solar light within 90 min at a concentration of 140 ppm of diclofenac. On the contrary,  
39 HDTMA-M-BiPO<sub>4</sub> shows an oxidation rate of only 22 % under the same conditions. It was deduced  
40 that the strong surface interactions between HDTMA and BiPO<sub>4</sub> coated on smectite can form a strong  
41 interfacial bridge which boosts the visible light response and the separation of photogenerated  
42 charges.

43 **Keywords:** Interfacial interaction, HDTMA-BiPO<sub>4</sub>, Heterostructures, Solar photocatalysis, Water  
44 remediation.

45

## 46 **Introduction**

47 TiO<sub>2</sub> photocatalysis, since it is discovered in 1972 by Fujishima and Honda [1], has passed by  
48 extensive fundamental research and technology pathways towards environmental remediation and  
49 energy production [2-6]. The photocatalytic materials fabrication side has taken the most of such  
50 scientific and technological research advancements, and many types of photocatalytic materials have  
51 been suggested within the last decades [7-12]. Even with such a pool of reported research over more  
52 than 30 years, photocatalytic technology is still not convincing enough to be applied extensively in  
53 real-world due to many technological and economic issues. Shortly, to convince the scientific  
54 community to invest in photocatalytic technology, several issues should be pointed out, including the  
55 efficiency of the photocatalytic system compared to existing technologies for a given application, the  
56 cost and sustainability of the system. In terms of water purification via the photocatalytic process,  
57 many benefits and weaknesses have been raised recently, putting the photocatalytic technology under  
58 huge criticisms. Advantages of photocatalysis can involve using solar light as a free energy resource  
59 to purify the water on sunny days/regions in a quasi-continuous economic way. However, a correct  
60 application should be found to use photocatalysis since this technology is applicable under limited  
61 conditions (i.e., less dense wastewaters) because of the use of light to activate the photocatalysts.  
62 Based on the reported research, photocatalytic technology has shown low mass transfer (primarily  
63 when naked semiconductors are used), generation of by-products, surface deactivation, and  
64 complicated or/and expensive synthesis of materials, and so on, as discussed recently by Djellabi et  
65 al. [13]. For better technology transfer, several approaches have been suggested to overcome such  
66 drawbacks. One of them, the combination of photocatalytic semiconductors with highly adsorptive  
67 materials, has been considered as a successful approach. In such a combination, several unique  
68 characteristics can be obtained as follows: (i): the coating of small nanoparticles (NPs) of  
69 semiconductors on the large particle of adsorbent solves the problem of hard recovery of NPs after  
70 the treatment. (ii): The photocatalytic action of NPs on the surface of adsorbent can limit the fast

71 saturation since the oxidative by photogenerated reactive oxygen species (ROSs) reduces the content  
72 of pollutants and liberates different adsorptive sites. (iii): Unlike naked semiconductors, the  
73 photogenerated by-products can be adsorbed on the surface for further oxidation, avoiding their  
74 toxicity in water. (iv): visible light response of semiconductors can be improved when they are  
75 hybridized with some adsorptive materials due to the photosensitizing or surface interactions [14, 15].  
76 Synergism between the photocatalytic activity and the adsorption effect can be found, wherein a  
77 cooperative mechanism, so-called Adsorb and Shuttle process, can take place to remove the pollutants  
78 even at higher concentrations [16, 17].

79 Bismuth phosphate ( $\text{BiPO}_4$ ), a relatively newly emerging photocatalyst, which was used for the first  
80 time in 2010 [18], has been reported to be very effective towards the oxidation of organic pollutants  
81 due to its more positive valance band compared to the common  $\text{TiO}_2$ , allowing better oxidation of  
82 water molecules into a high yield of hydroxyl radicals. However,  $\text{BiPO}_4$  exhibits a large bandgap (in  
83 the range of 3.5–4.6 eV), and it requires a strong UV light irradiation to be activated. Loeb *et al.*  
84 reported in their critical review [19] that  $\text{BiPO}_4$  could be a great alternative photocatalyst for the  
85 oxidation and mineralization of organic pollutants. At the same time, creative and yet-to-be-devised  
86 approaches to fix its drawbacks are needed to benefit from this promising photocatalyst for its use in  
87 photocatalytic wastewater treatment. Several approaches have been already reported to enhance the  
88 adsorption ability and visible light response of  $\text{BiPO}_4$  such as doping [20-22], heterojunction systems  
89 [23-25], oxygen vacancy [26-29], phase junction [30-32], and combination with  $\pi$ -conjugated  
90 materials [33-35].

91 In the present work, the enhancement of the ability of  $\text{BiPO}_4$  was carried out via the hybridization  
92 with two clays (smectite and montmorillonite) to enhance its adsorption capacity and photoactivity  
93 under UV and solar light towards the oxidation of diclofenac. To further improve the performance of  
94  $\text{BiPO}_4$ -clay based photocatalysts, hexadecyl trimethyl ammonium bromide (HDTMA) was used to  
95 modify the clay before the coating of  $\text{BiPO}_4$ . The role of HDTMA in enhancing the adsorption and

96 photocatalytic abilities was investigated. Finally, the optimization of BiPO<sub>4</sub> amount coated on the  
97 surface HDTMA modified smectite was studied to figure out the ratio of BiPO<sub>4</sub> towards the  
98 adsorption and photoactivity.

## 99 **2. Materials and methods**

### 100 **2.1. Synthesis of photocatalysts**

101 The raw montmorillonite used in this study was obtained from Roussel deposit in Maghnia (Algeria).  
102 Its cationic exchange capacity is 89.30 mmol/100 g. The raw smectite is gray clay derived from Djebel  
103 haidoudi near El hamma, and it exhibits a cation exchange capacity of 64.28 meq/100 g. The  
104 fabrication of Montmorillonite-BiPO<sub>4</sub> (M- BiPO<sub>4</sub>) was carried out by simple precipitation of BiNO<sub>3</sub>  
105 and NaH<sub>2</sub>PO<sub>4</sub> on the surface of Montmorillonite. For this purpose, 1 g of montmorillonite is spread  
106 in 20 mL ultrapure water and sonicated for 20 min. Then, under stirring, 5 mL of BiNO<sub>3</sub> (0.3 M) is  
107 added dropwise into montmorillonite mixture and left for 60 min under stirring at 60°C. After that, 5  
108 mL of NaH<sub>2</sub>PO<sub>4</sub> (0.3 M) is added dropwise into the mixture, and stirred for 2 h. The obtained solid  
109 was washed and dried at 120°C for a night. HTDMA-Montmorillonite (HTDMA-M) and HTDMA-  
110 smectite (HTDMA-S) were prepared by adding a desired amount of HTDMA to water-  
111 montmorillonite or smectite, followed by microwave treatment. The sample was recovered and dried  
112 at 120 for a night. HTDMA-M-BiPO<sub>4</sub> and HTDMA-S-BiPO<sub>4</sub> were prepared by precipitation of  
113 BiNO<sub>3</sub> and NaH<sub>2</sub>PO<sub>4</sub> as described above. Bare BiPO<sub>4</sub> was also prepared for the comparison.

### 114 **2.2. Characterization**

115 Fourier transform infrared spectroscopy analyses (FT-IR) analysis on the as-prepared samples was  
116 carried out using a Bruker Vertex 70 spectrophotometer (Bruker, Billerica, MA, US). XRD spectra  
117 of samples were recorded on a PANalytical X'PERT-PRO diffractometer with monochromatic CuK $\alpha$   
118 radiation ( $\lambda = 1.54056 \text{ \AA}$ ). X-ray photoelectron spectra (XPS) were recorded on a XPS PHI Quantum

119 instrument. UV–Vis absorption spectra were recorded in the wavelength range of 300–800 nm on  
120 Cary 5000 UV-Vis spectrophotometer (Agilent Technology).

### 121 **2.3. Adsorption and photocatalytic tests**

122 The efficiency of as-prepared photocatalysts was tested against the photocatalytic oxidation of  
123 diclofenac under UV ( $\lambda_{\text{max}} = 365 \text{ nm}$ ,  $100 \text{ W/m}^2$ ) and solar light ( $35 \text{ W}\cdot\text{m}^{-2}$ , ULTRA VITALUX 300  
124 W-OSRAM, OSRAM, München, Germany) irradiations. Dark and photolysis experiments were carried  
125 out for the purpose of comparison. At different time intervals, samples were collected and filtered  
126 using filter paper of  $0.45 \mu\text{m}$  diameter. The analysis of diclofenac was performed using a UV-vis  
127 spectrophotometer at a wavelength of 276 nm.

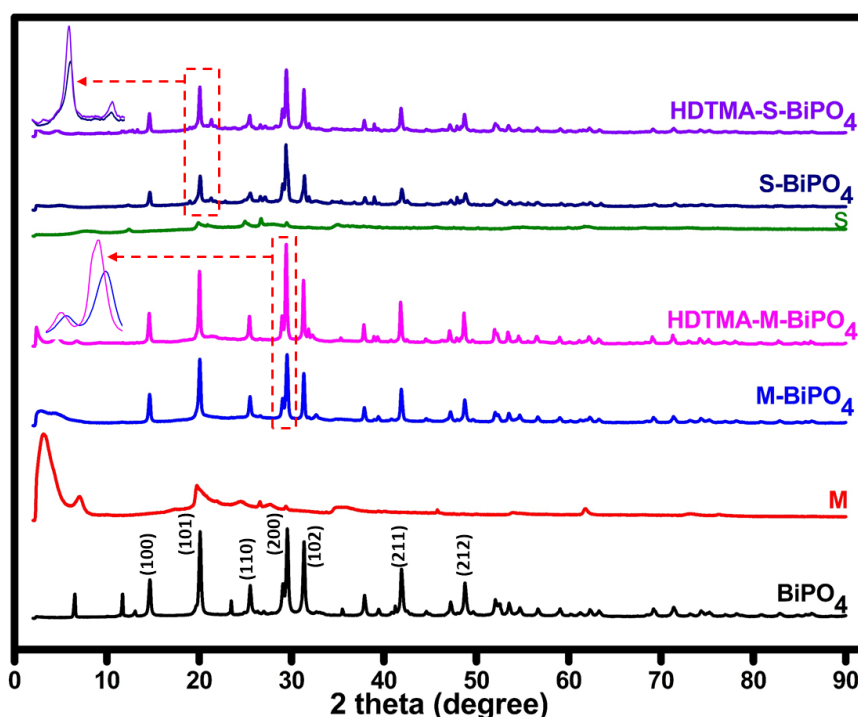
## 128 **3. Results and discussion**

### 129 **3.1. Characterization of materials**

130 XRD patterns of  $\text{BiPO}_4$ , M, M- $\text{BiPO}_4$ , HDTMA-M- $\text{BiPO}_4$ , S, S- $\text{BiPO}_4$  and HDTMA-M- $\text{BiPO}_4$   
131 samples are shown in **Figure 1**. In  $\text{BiPO}_4$  and all  $\text{BiPO}_4$  modified clays, diffraction peaks were  
132 appeared at around  $14.7$ ,  $20.1$ ,  $25.5$ ,  $29.5$ ,  $31.3$ ,  $41.9$ , and  $48.7^\circ$  which fit with the crystal orientations  
133 of the hexagonal phase of  $\text{BiPO}_4$  (space group: P3121(152), JCPDS, card no. 15-0766) [36].  
134 Montmorillonite's XRD pattern shows a strong d(100) basal spacing reflection at around  $2\theta = 5.87^\circ$   
135 [37]. However, after the coating of  $\text{BiPO}_4$  on the surface of M, this peak was reduced significantly,  
136 confirming the formation of  $\text{BiPO}_4$  nanoparticles between the montmorillonite layers. The bare  
137 smectite pattern does not show a strong basal spacing diffraction peak compared to the  
138 montmorillonite sample. The coating of  $\text{BiPO}_4$  on HDTMA modified clays resulted in stronger  
139 intensities of  $\text{BiPO}_4$  diffraction peaks. This may be due to the better crystallization and distribution  
140 of  $\text{BiPO}_4$  nanoparticles on the surface of HDTMA-clays. The HDTMA organic fragments can interact  
141 between the layers of the clay, and also it may react with the components of the clay on the external  
142 surface. It may be deduced that the clays with larger basal spacing can receive HDTMA organic  
143 fragments compared to those with lower basal spacing. Therefore, the introduction of  $\text{BiPO}_4$  on

144 HDTMA modified clays having different basal spacing could have different manners. It is expected  
145 that the  $\text{BiPO}_4$  could be accumulated in the basal spacing of montmorillonite, while  $\text{BiPO}_4$  might be  
146 mostly coated on the external surface of smectite because of its low basal spacing.

147 **Figure 2** shows FTIR curves of different samples. In bare  $\text{BiPO}_4$ , the large band at  $750\text{-}1200\text{ cm}^{-1}$  is  
148 assigned to the characteristic asymmetric stretching modes of P–O bonds of  $\text{PO}_4^{3-}$  [38]. Peaks at the  
149 range  $520\text{-}600\text{ cm}^{-1}$  are due to the bending vibrations of O–P–O linkage. Characteristic peaks of  
150  $\text{BiPO}_4$  were not very obvious in  $\text{BiPO}_4$  modified clay samples, which could be overlapped with the  
151 original peaks since both montmorillonite and smectite clays have absorption peaks at the same area,  
152 i.e., the band at around  $1000\text{ cm}^{-1}$  and around  $600\text{ cm}^{-1}$  is due to Si–O stretching in-plane and Al–O–  
153 Si deformation, respectively [37, 39]. FTIR confirmed the fixation of HTDMA in HDTMA–M– $\text{BiPO}_4$ ,  
154 S, S– $\text{BiPO}_4$ , and HDTMA–M– $\text{BiPO}_4$  samples curves, wherein two peaks at around  $2936$  and  $2871\text{ cm}^{-1}$   
155 <sup>1</sup> were appeared due to the presence of  $\text{CH}_2$  and  $\text{CH}_3$ , respectively [40].

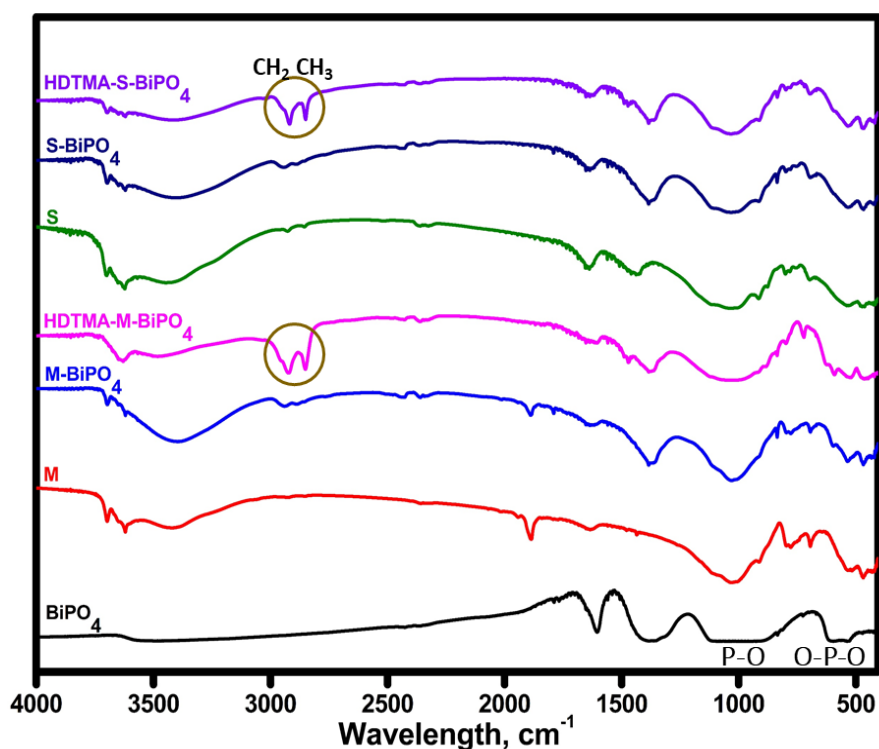


156

157 **Figure 1.** XRD patterns of  $\text{BiPO}_4$ , M, M– $\text{BiPO}_4$ , HDTMA–M– $\text{BiPO}_4$ , S, S– $\text{BiPO}_4$  and HDTMA–S–

158

$\text{BiPO}_4$  samples.



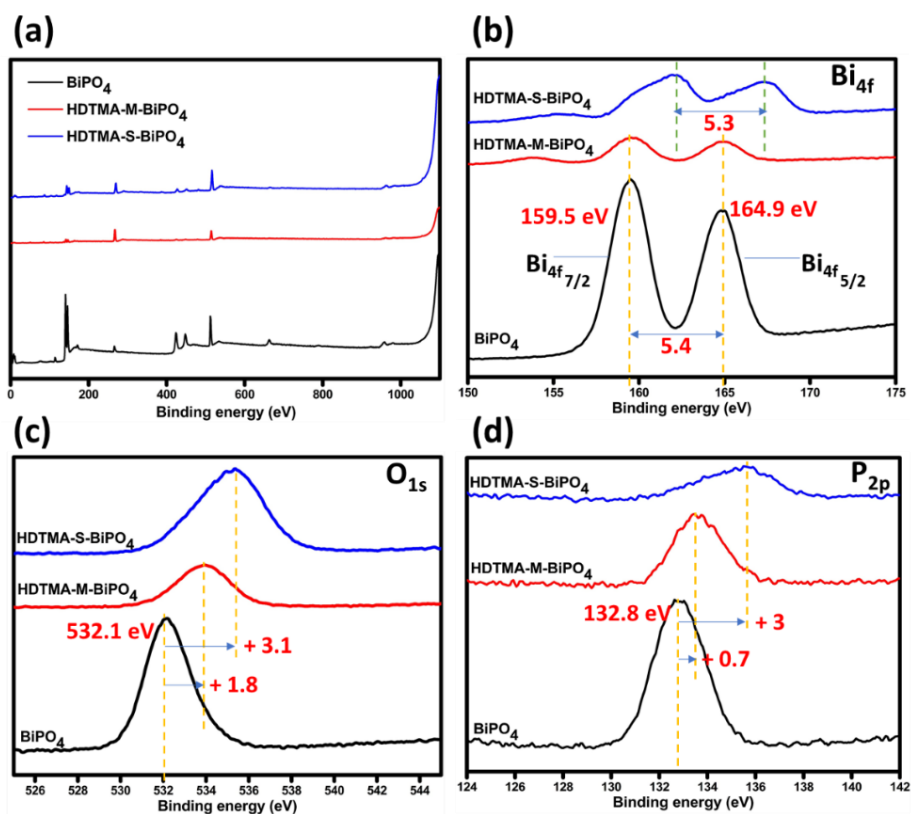
159

160 **Figure 2.** FTIR spectra of BiPO<sub>4</sub>, M, M-BiPO<sub>4</sub>, HDTMA-M-BiPO<sub>4</sub>, S, S-BiPO<sub>4</sub> and HDTMA-S-  
 161 BiPO<sub>4</sub> samples.

162 The results of XPS analysis carried out on BiPO<sub>4</sub>, HDTMA-M-BiPO<sub>4</sub>, and HDTMA-S-BiPO<sub>4</sub>  
 163 samples are shown in **Figure 3**. In terms of Bi<sub>4f</sub> high resolution (**Figure 3,b**), BiPO<sub>4</sub> profile shows  
 164 two intense peaks at 159.5 and 164.9 eV, which are due to Bi<sub>4f7/2</sub> and Bi<sub>4f5/2</sub>, respectively, showing  
 165 the trivalent oxidation state of Bi species [41]. The distance between Bi<sub>4f7/2</sub> and Bi<sub>4f5/2</sub> was calculated  
 166 to be 5.3 eV. The position of these peaks was not affected in the case of HDTMA-M-BiPO<sub>4</sub>, but a  
 167 significant change in the intensity is observed because of the low quantity of BiPO<sub>4</sub>. In the case of  
 168 HDTMA-S-BiPO<sub>4</sub>, a huge change in Bi<sub>4f</sub> peaks was recorded. The shape of peaks was deformed  
 169 along with a significant shift towards higher binding energies. The peaks shifting was about 1.3 eV,  
 170 while the distance between Bi<sub>4f7/2</sub> and Bi<sub>4f5/2</sub> was reduced to 5.3 eV. Such a change proves the strong  
 171 interactions between the atoms of BiPO<sub>4</sub> and the components of HDTMA-S. **Figure 3,c** shows O<sub>1s</sub>  
 172 profiles in BiPO<sub>4</sub>, HDTMA-M-BiPO<sub>4</sub> and HDTMA-S-BiPO<sub>4</sub>. Bare BiPO<sub>4</sub> shows a single peak at  
 173 532.2 eV assigned to crystalline oxygen [42]. O<sub>1s</sub> spectra in HDTMA-M-BiPO<sub>4</sub> and HDTMA-S-

174 BiPO<sub>4</sub> show a significant shifting towards higher binding energies by around 1.8 and 3.1 eV,  
175 respectively, which might be due to the adsorbed oxygen and the chemical interactions between  
176 crystalline O<sup>2-</sup> of BiPO<sub>4</sub> and HDTMA-clay supports. The P<sub>2p</sub> of PO<sub>4</sub><sup>3-</sup> state was appeared at a binding  
177 energy of 132.8 eV in bare BiPO<sub>4</sub> [43], while a notable shift towards higher energies by 0.7 and 3 eV  
178 was detected in HDTMA-M-BiPO<sub>4</sub> and HDTMA-S-BiPO<sub>4</sub> samples, respectively. The observed peaks  
179 shifting in HDTMA-M-BiPO<sub>4</sub> and HDTMA-S-BiPO<sub>4</sub> reflects the migration of electron density of  
180 BiPO<sub>4</sub> to HDTMA-clay components and the formation of a built-in electric field at the interface. It is  
181 important to point out that the XPS peak shifting in HDTMA-S-BiPO<sub>4</sub> is more evident than HDTMA-  
182 M-BiPO<sub>4</sub>, suggesting that the characteristics of clays play an important role in forming the surface  
183 interactions. In fact, from XRD patterns, it can be seen that M samples exhibit a strong interlayer d-  
184 spacing ( $2\theta = 5.87^\circ$ ), wherein, BiPO<sub>4</sub> particles can be introduced and fixed inside the interlayers, as  
185 confirmed by the XRD pattern of M-BiPO<sub>4</sub> (significant reduction  $2\theta = 5.87^\circ$  in peak). However, in  
186 terms of the S sample, BiPO<sub>4</sub> might be fixed on the external surface due to the low interlayer spacing,  
187 which allows the interaction with the added HDTMA to form more interactions and heterostructure.  
188 The optical properties of samples were estimated by UV–Vis diffuse reflectance (Figure 4). Respect  
189 to bare BiPO<sub>4</sub>, all samples showed a red-shift in the absorption edge. The band gaps of BiPO<sub>4</sub>,  
190 HDTMA-S-BiPO<sub>4</sub> and HDTMA-M-BiPO<sub>4</sub> were estimated about 3.87, 2.75 and 2.60 eV, respectively.  
191 Interestingly, samples with HDTMA showed as well an ulterior peak centrated at around 380 nm  
192 which proves the formation of heterojunction system that would boost further the absorption of light  
193 and the photosensitization effect.

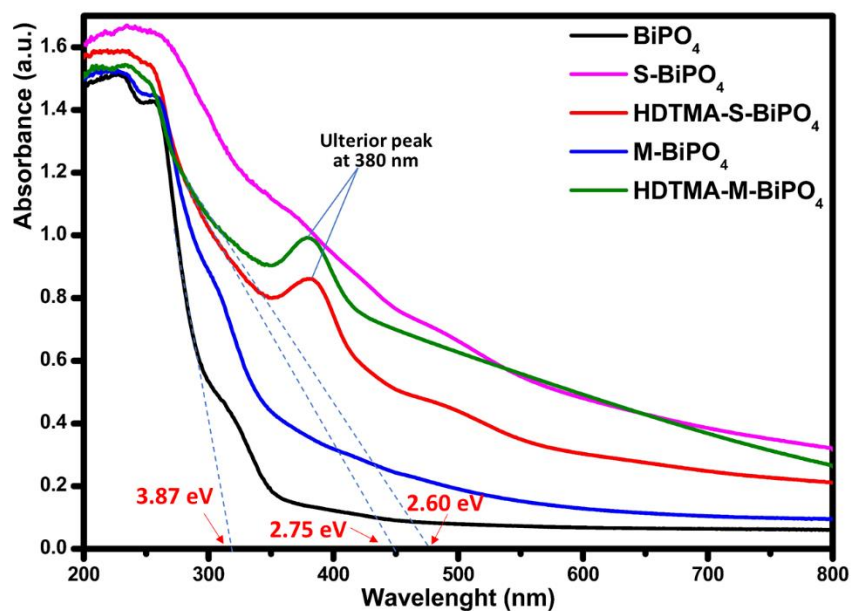
194



195

196 **Figure 3.** (a): XPS survey spectra of  $\text{BiPO}_4$ , HDTMA-M- $\text{BiPO}_4$ , and HDTMA-S- $\text{BiPO}_4$  samples.

197 (b):  $\text{Bi}4f$  high-resolution profiles. (c):  $\text{O}1s$  high-resolution profiles. (d):  $\text{P}2p$  high-resolution profiles.

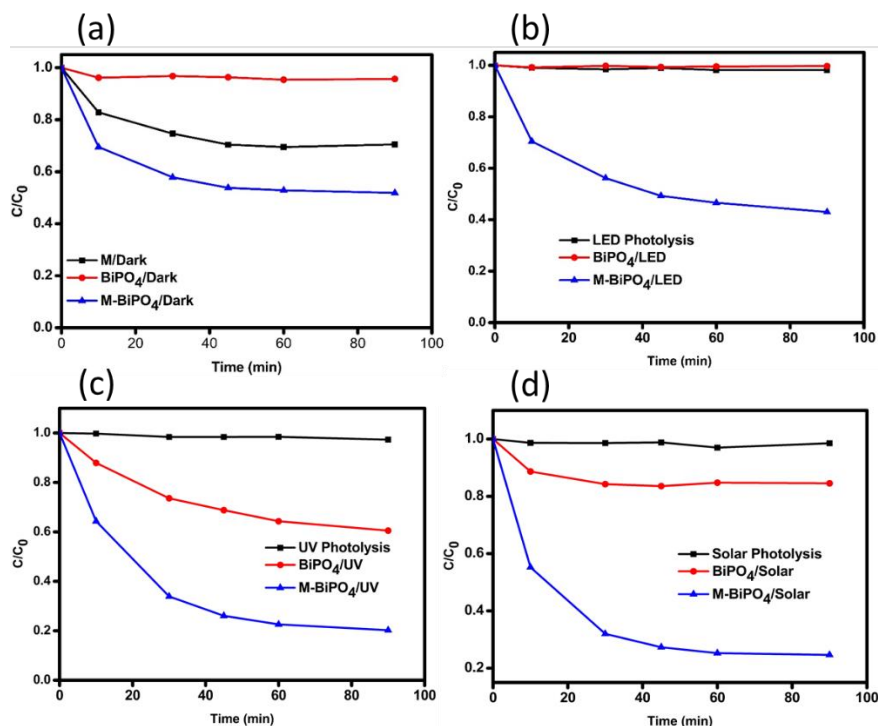


198

199 **Figure 4.** UV-Vis diffuse reflectance spectra of bare  $\text{BiPO}_4$ , S- $\text{BiPO}_4$ , HDTMA-S- $\text{BiPO}_4$ , M- $\text{BiPO}_4$   
 200 and HDTMA-M- $\text{BiPO}_4$ .

### 201 3.2. Photocatalytic activity

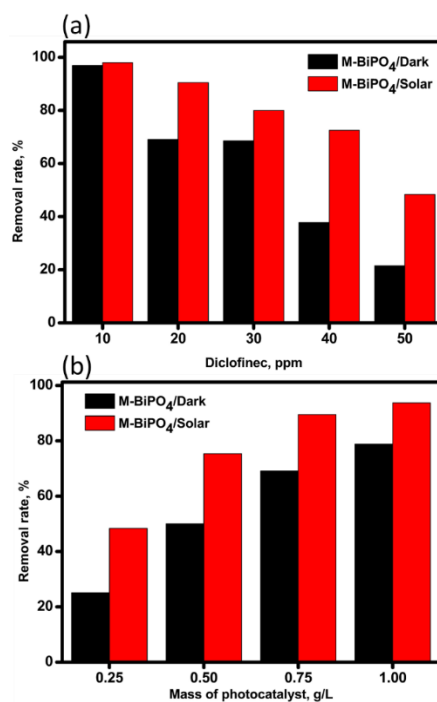
202 The adsorption and photoactivity of bare BiPO<sub>4</sub> and M-BiPO<sub>4</sub> under LED, UV, and solar light were  
203 tested comparatively, and the results are shown in **Figure 5**. From **Figure 5.a**, it can be noticed that  
204 the coating of BiPO<sub>4</sub> on the M surface led to enhanced adsorption ability compared to bare M and  
205 BiPO<sub>4</sub>, which could be due to the formation of novel surface adsorption sites. Under LED light  
206 irradiation (**Figure 5.b**), no photocatalytic activity was observed using bare BiPO<sub>4</sub>, while it can be  
207 seen that M- BiPO<sub>4</sub> has a slight photocatalytic activity under light. It is expected that bare BiPO<sub>4</sub> is  
208 not photoactive under visible light due to its large bandgap. However, its hybridization with the  
209 montmorillonite by in situ precipitation might lead to form chemical interactions with the  
210 components, as shown in XPS spectra. Under UV light (**Figure 5. c**), bare BiPO<sub>4</sub> shows a modest  
211 photocatalytic activity, wherein less than 40 % diclofenac was removed. On the other hand, M-BiPO<sub>4</sub>  
212 shows much better photocatalytic oxidation under UV light of diclofenac, more than 80 % within 90  
213 min. The reasons behind the enhanced removal of diclofenac under UV is undoubtedly due to the  
214 combination of adsorption and photocatalytic activity in the same platform, wherein the adsorb & and  
215 shuttle process can accelerate the photooxidation of diclofenac. The adsorptive domain (M) acts to  
216 concentrate the diclofenac molecules on the surface nearby the photoactive BiPO<sub>4</sub>, resulting in fast  
217 oxidation by photogenerated ROSs [16]. Indeed, the bridge between the surface of M and BiPO<sub>4</sub>  
218 might help to enhance the generation of ROSs due to the better e<sup>-</sup>/h<sup>+</sup> charges separation. Remarkably,  
219 M- BiPO<sub>4</sub> showed excellent photoactivity under solar light, which could be due to the self-doping of  
220 BiPO<sub>4</sub> or structure modification during the precipitation of BiPO<sub>4</sub> on the surface of M. Bonds between  
221 BiPO<sub>4</sub> and M might lead to decrease the bandgap and promotes the charge generation and separation.



222

223 **Figure 5.** (a): Adsorption of diclofenac by bare M, BiPO<sub>4</sub>, and M- BiPO<sub>4</sub>, (b): photolysis and  
 224 photocatalytic oxidation of diclofenac under LED irradiation by BiPO<sub>4</sub> and M- BiPO<sub>4</sub>, (c): photolysis  
 225 and photocatalytic oxidation of diclofenac under UV irradiation by BiPO<sub>4</sub> and M- BiPO<sub>4</sub>, (d):  
 226 photolysis and photocatalytic oxidation of diclofenac under solar irradiation by BiPO<sub>4</sub> and M- BiPO<sub>4</sub>.  
 227 [Photocatalyst]: 0.5 g/L, [Diclofenac]: 20 ppm.

228 To further evaluate the adsorption/photocatalytic synergism in M-BiPO<sub>4</sub> photocatalyst, adsorption  
 229 and solar photocatalytic experiments were carried out with different diclofenac concentrations and  
 230 different M-BiPO<sub>4</sub> masses. As depicted in **Figure 6.a**, at lower concentrations, the adsorption process  
 231 is predominant compared to the photocatalytic oxidation. The more the diclofenac concentration is,  
 232 the more photocatalytic oxidation is evident. At concentrations of 40 and 50 ppm, the removal of  
 233 diclofenac by photocatalytic effect is pronounced. The behavior of the M-BiPO<sub>4</sub> at different masses  
 234 (**Figure 6.b**) shows that the more the mass of photocatalyst is, the more adsorption of diclofenac is  
 235 obtained. It is important to mention that the photocatalytic effect, in such a type of materials, has  
 236 another advantage compared to simple adsorption, which is the self-cleaning of the surface for further  
 237 adsorption, which in turn retards the fast saturation of the material.

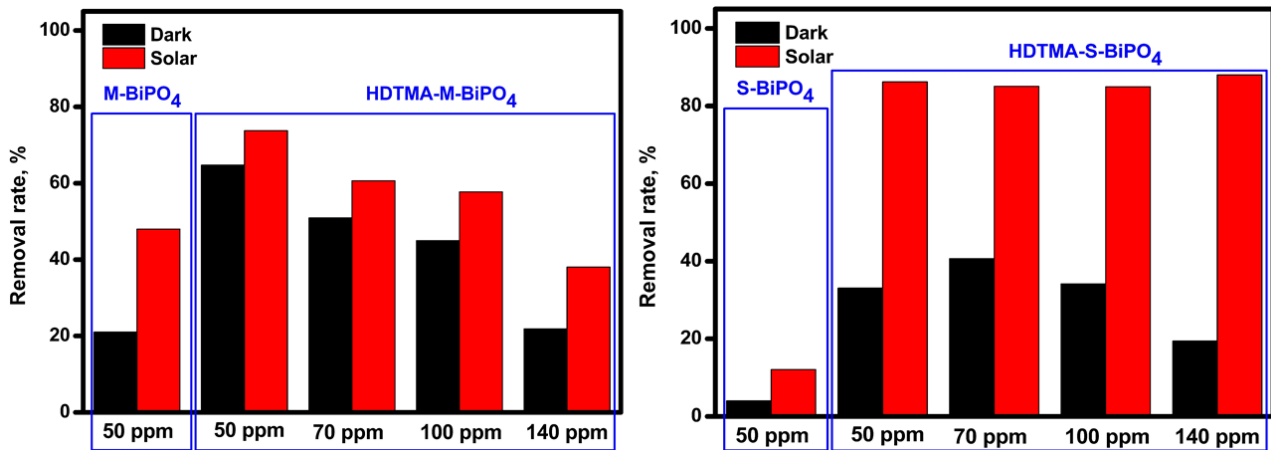


238

239 **Figure 6.** (a): Effect of diclofenac concentration on the adsorption and photocatalytic activity under  
 240 solar light. [Photocatalyst]: 0.75 g/L, contact time 90 min. (b): Effect of photocatalyst mass on the  
 241 removal of diclofenac by adsorption and photocatalytic activity under solar light, [diclofenac]: 20  
 242 ppm, contact time 90 min.

243 To investigate the role of HDTMA and the type of clay support, HDTMA-M-BiPO<sub>4</sub> and HDTMA-  
 244 S-BiPO<sub>4</sub> were fabricated, and their photocatalytic activities were evaluated at different diclofenac  
 245 concentrations ranging from 50 ppm to 140 ppm (**Figure 7**). Firstly, the photocatalytic tests showed  
 246 that M-BiPO<sub>4</sub> exhibits higher photocatalytic activity under solar light compared to S-BiPO<sub>4</sub> at a  
 247 concentration of 50 ppm. In this case, M-BiPO<sub>4</sub> might have better porosity and photoactivity as  
 248 compared to the S-BiPO<sub>4</sub> sample. The fixation of BiPO<sub>4</sub> on the montmorillonite, which has an  
 249 excellent basal spacing, allows a better distribution of BiPO<sub>4</sub> particles. It can be seen in XRD patterns  
 250 (**Figure 1**) that the peaks in M-BiPO<sub>4</sub> are more intense than those in S-BiPO<sub>4</sub>. In addition, since M-  
 251 BiPO<sub>4</sub> has better adsorption ability, a higher photoactivity is expected by adsorb and shuttle means  
 252 [44, 45]. However, the introduction of HDTMA to the surface of montmorillonite and smectite before  
 253 the coating of BiPO<sub>4</sub> has changed the manner completely. In terms of HDTMA-M-BiPO<sub>4</sub>, the

254 adsorption ability of the composite was significantly enhanced, leading to faster removal of  
255 diclofenac. It can also be seen that the adsorption is predominant in the photocatalytic action in  
256 HDTMA-M-BiPO<sub>4</sub> system, especially at a concentration ranging from 50 to 100 ppm. The removal  
257 rates decrease as a function of diclofenac concentration. It might be deduced the enhancement in the  
258 effectiveness of HDTMA-M-BiPO<sub>4</sub> is more due to the adsorb and shuttle process that can be appeared  
259 in the platform of this material, which improves the concentration of diclofenac molecules on the  
260 surface near the photoactive BiPO<sub>4</sub>. On top of that, the photocatalytic activity of BiPO<sub>4</sub> fixed on the  
261 surface of montmorillonite might also be improved through chemical interactions with HDTMA. In  
262 the case of HDTMA-S-BiPO<sub>4</sub>, another surprising manner was found. HDTMA has notably enhanced  
263 the adsorption ability of the composite, but it has a major role for photocatalytic activity under solar  
264 light. The removal of diclofenac under solar light was high even at higher concentrations, by  
265 photocatalytic means as a predominant action, unlike HDTMA-S-BiPO<sub>4</sub>. Based on these results and  
266 XPS analysis, it might be deduced that the photocatalytic activity in HDTMA-S-BiPO<sub>4</sub> under solar  
267 light is assigned to the strong interface interactions between BiPO<sub>4</sub> and HDTMA, forming a  
268 heterostructure platform. A better visible light response and an enhanced photoproduced charges  
269 separation can be found in the HDTMA-S-BiPO<sub>4</sub> surface because of the interface junction. As a  
270 result, a higher yield of reactive oxygen species can be produced in the medium. BiPO<sub>4</sub> is an excellent  
271 producer of hydroxyl radicals, compared to common photocatalysts (i.e., TiO<sub>2</sub>), because of its more  
272 positive valance band. However, this photocatalyst requires surface modification to decrease its  
273 bandgap and improve the separation of e<sup>-</sup>/h<sup>+</sup> charge carriers. Interestingly, the hybridization of BiPO<sub>4</sub>  
274 and HDTMA in our conditions had solved perfectly such structure drawbacks.



275

276 **Figure 7.** Adsorption and photocatalytic oxidation of diclofenac by BiPO<sub>4</sub> modified clays and BiPO<sub>4</sub>  
 277 modified HDTMA-clays, at different diclofenac concentrations. [Photocatalyst]: 0.375 g/L, contact  
 278 time 90 min.

#### 279 4. Conclusions

280 The results of this investigation show the significant role of the co-hybridization of BiPO<sub>4</sub> and  
 281 HDTMA on the surface of clays, namely, montmorillonite and smectite. In the first study, it was  
 282 found out that the coating of BiPO<sub>4</sub> on the surface of montmorillonite leads enhanced adsorption and  
 283 photocatalytic activity for the oxidation of diclofenac under LED, UV, and solar light irradiations.  
 284 Compared to M- BiPO<sub>4</sub>, S-BiPO<sub>4</sub> was less efficient in adsorption and photocatalytic activity under  
 285 solar light. Such a difference in the effectiveness might be due to the different basal spacing of the  
 286 original clay material, having the montmorillonite an extra-large basal spacing compared to smectite.  
 287 The co-modification of clays by BiPO<sub>4</sub> and HDTMA has shown interesting results in terms of  
 288 interface interactions. HDTMA in HDTMA-M-BiPO<sub>4</sub> had a positive effect of improving further the  
 289 adsorption ability and the photoactivity, wherein diclofenac was removed mostly by physical  
 290 adsorption. However, in HDTMA-S-BiPO<sub>4</sub> composite, HDTMA has enhanced the adsorption ability  
 291 from one side. Still, mostly HDTMA has improved the photoactivity of BiPO<sub>4</sub> dramatically by  
 292 forming an interfacial bridge, confirmed by XPS analysis, which leads to excellent photoexcitation

293 and separation of charges carries. This study showed promising results in enhancing the adsorption  
294 and photoactivity abilities of clay-BiPO<sub>4</sub> by sustainable and straightforward surface modification.

## 295 **References**

296 [1] A. Fujishima, K. Honda, Electrochemical photolysis of water at a semiconductor electrode, *nature*,  
297 238 (1972) 37-38.

298 [2] J. Luo, S. Zhang, M. Sun, L. Yang, S. Luo, J.C. Crittenden, A critical review on energy conversion  
299 and environmental remediation of photocatalysts with remodeling crystal lattice, surface, and  
300 interface, *ACS nano*, 13 (2019) 9811-9840.

301 [3] A. Rani, R. Reddy, U. Sharma, P. Mukherjee, P. Mishra, A. Kuila, L.C. Sim, P. Saravanan, A  
302 review on the progress of nanostructure materials for energy harnessing and environmental  
303 remediation, *Journal of Nanostructure in Chemistry*, 8 (2018) 255-291.

304 [4] K. Kabra, R. Chaudhary, R.L. Sawhney, Treatment of hazardous organic and inorganic  
305 compounds through aqueous-phase photocatalysis: a review, *Industrial & engineering chemistry*  
306 *research*, 43 (2004) 7683-7696.

307 [5] A.A. Ismail, D.W. Bahnemann, Photochemical splitting of water for hydrogen production by  
308 photocatalysis: A review, *Solar energy materials and solar cells*, 128 (2014) 85-101.

309 [6] K. Perović, M. Kovačić, H. Kušić, U.L. Štangar, F. Fresno, D.D. Dionysiou, A. Loncaric Bozic,  
310 Recent achievements in development of TiO<sub>2</sub>-based composite photocatalytic materials for solar  
311 driven water purification and water splitting, *Materials*, 13 (2020) 1338.

312 [7] R. Djellabi, M.F. Ordonez, F. Conte, E. Falletta, C.L. Bianchi, I. Rossetti, A Review of Advances  
313 in Multifunctional XTiO<sub>3</sub> Perovskite-type Oxides as piezo-photocatalysts for Environmental  
314 Remediation and Energy Production, *Journal of Hazardous Materials*, (2021) 126792.

315 [8] M.G. Alalm, R. Djellabi, D. Meroni, C. Pirola, C.L. Bianchi, D.C. Boffito, Toward Scaling-Up  
316 Photocatalytic Process for Multiphase Environmental Applications, *Catalysts*, 11 (2021) 562.

- 317 [9] T. Hisatomi, J. Kubota, K. Domen, Recent advances in semiconductors for photocatalytic and  
318 photoelectrochemical water splitting, *Chemical Society Reviews*, 43 (2014) 7520-7535.
- 319 [10] C. Xu, P.R. Anusuyadevi, C. Aymonier, R. Luque, S. Marre, Nanostructured materials for  
320 photocatalysis, *Chemical Society Reviews*, 48 (2019) 3868-3902.
- 321 [11] J. Low, J. Yu, M. Jaroniec, S. Wageh, A.A. Al-Ghamdi, Heterojunction photocatalysts,  
322 *Advanced materials*, 29 (2017) 1601694.
- 323 [12] R. Djellabi, C.L. Bianchi, M.R. Haider, J. Ali, E. Falletta, M.F. Ordonez, A. Bruni, M. Sartirana,  
324 R. Geioushy, Photoactive Polymer for Wastewater Treatment, *Nanomaterials for Water Treatment  
325 and Remediation*, CRC Press2021, pp. 217-244.
- 326 [13] R. Djellabi, R. Giannantonio, E. Falletta, C.L. Bianchi, SWOT analysis of photocatalytic  
327 materials towards large scale environmental remediation, *Current Opinion in Chemical Engineering*,  
328 33 (2021) 100696.
- 329 [14] R. Djellabi, B. Yang, Y. Wang, X. Cui, X. Zhao, Carbonaceous biomass-titania composites with  
330 TiOC bonding bridge for efficient photocatalytic reduction of Cr (VI) under narrow visible light,  
331 *Chemical Engineering Journal*, 366 (2019) 172-180.
- 332 [15] R. Djellabi, B. Yang, K. Xiao, Y. Gong, D. Cao, H.M.A. Sharif, X. Zhao, C. Zhu, J. Zhang,  
333 Unravelling the mechanistic role of TiOC bonding bridge at titania/lignocellulosic biomass interface  
334 for Cr (VI) photoreduction under visible light, *Journal of colloid and interface science*, 553 (2019)  
335 409-417.
- 336 [16] A.N. Saber, R. Djellabi, I. Fellah, N. Abderrahim, C.L. Bianchi, Synergistic sorption/photo-  
337 Fenton removal of typical substituted and parent polycyclic aromatic hydrocarbons from coking  
338 wastewater over CuO-Montmorillonite, *Journal of Water Process Engineering*, 44 (2021) 102377.
- 339 [17] R. Djellabi, M.F. Ghorab, A. Smara, C.L. Bianchi, G. Cerrato, X. Zhao, B. Yang, Titania-  
340 Montmorillonite for the photocatalytic removal of contaminants from water: adsorb & shuttle process,  
341 *Green materials for wastewater treatment*, Springer2020, pp. 291-319.

342 [18] C. Pan, Y. Zhu, New type of BiPO<sub>4</sub> oxy-acid salt photocatalyst with high photocatalytic activity  
343 on degradation of dye, *Environmental science & technology*, 44 (2010) 5570-5574.

344 [19] SK. Loeb, P.J. Alvarez, J.A. Brame, E.L. Cates, W. Choi, J. Crittenden, D.D. Dionysiou, Q. Li,  
345 G. Li-Puma, X. Quan, The technology horizon for photocatalytic water treatment: sunrise or sunset?,  
346 ACS Publications, 2018.

347 [20] J. Wang, N. Luo, S. Peng, L. Yang, M. Zhao, BiPO<sub>4</sub>: Ln<sup>3+</sup> (Ln= Eu, Tb, Eu/Tb) nanorods:  
348 room-temperature synthesis, reaction mechanism, and color-tunable emission, *Journal of Alloys and*  
349 *Compounds*, (2021) 162314.

350 [21] Y. Quan, X. Ji, K. Liu, C. Kang, Synthesis, characterization, and photocatalytic properties of La  
351 3+-doped BiPO<sub>4</sub> photocatalysts, *Kinetics and Catalysis*, 57 (2016) 207-211.

352 [22] D. Yu, X. Wu, G. Yan, J. Cao, Crystal phase, morphology evolution and luminescence properties  
353 of Eu<sup>3+</sup>-doped BiPO<sub>4</sub> phosphor prepared using the hydrothermal method, *Luminescence*, (2021).

354 [23] X. Ma, J. Hu, H. He, S. Dong, C. Huang, X. Chen, New understanding on enhanced  
355 photocatalytic activity of g-C<sub>3</sub>N<sub>4</sub>/BiPO<sub>4</sub> heterojunctions by effective interfacial coupling, *ACS*  
356 *Applied Nano Materials*, 1 (2018) 5507-5515.

357 [24] N. Sun, Y. Qu, C. Yang, Z. Yang, R. Yan, E. Wenyu, Z. Zhang, Z. Li, H. Li, I. Khan, Efficiently  
358 photocatalytic degradation of monochlorophenol on in-situ fabricated BiPO<sub>4</sub>/β-Bi<sub>2</sub>O<sub>3</sub> heterojunction  
359 microspheres and O<sub>2</sub>-free hole-induced selective dechlorination conversion with H<sub>2</sub> evolution,  
360 *Applied Catalysis B: Environmental*, 263 (2020) 118313.

361 [25] M. Yuan, T. Liu, Q. Shi, J. Dong, Understanding the KOH activation mechanism of zeolitic  
362 imidazolate framework-derived porous carbon and their corresponding furfural/acetic acid adsorption  
363 separation performance, *Chemical Engineering Journal*, 428 (2022) 132016.

364 [26] J. Xie, Y. Cao, D. Jia, Enhanced photocatalytic oxidizing ability via adjusting the band-edge  
365 position and oxygen defect concentration of bismuth phosphate, *Journal of Alloys and Compounds*,  
366 832 (2020) 154953.

367 [27] X. Zheng, J. Wang, J. Liu, Z. Wang, S. Chen, X. Fu, Photocatalytic degradation of benzene over  
368 different morphology BiPO<sub>4</sub>: revealing the significant contribution of high-energy facets and oxygen  
369 vacancies, *Applied Catalysis B: Environmental*, 243 (2019) 780-789.

370 [28] B. Shi, H. Yin, T. Li, J. Gong, S. Lv, Q. Nie, Synthesis of surface oxygen-deficient BiPO<sub>4</sub>  
371 nanocubes with enhanced visible light induced photocatalytic activity, *Materials Research*, 20 (2017)  
372 619-627.

373 [29] Y. Zhu, Q. Ling, Y. Liu, H. Wang, Y. Zhu, Photocatalytic performance of BiPO<sub>4</sub> nanorods  
374 adjusted via defects, *Applied Catalysis B: Environmental*, 187 (2016) 204-211.

375 [30] A.B. Azzam, S. El-Sheikh, R. Geioushy, BA. Salah, M. Farida, ASS Helal, Facile fabrication of  
376 a novel BiPO<sub>4</sub> phase junction with enhanced photocatalytic performance towards aniline blue  
377 degradation, *RSC advances*, 9 (2019) 17246-17253.

378 [31] Y. Guo, P. Wang, J. Qian, Y. Ao, C. Wang, J. Hou, Phosphate group grafted twinned BiPO<sub>4</sub>  
379 with significantly enhanced photocatalytic activity: Synergistic effect of improved charge separation  
380 efficiency and redox ability, *Applied Catalysis B: Environmental*, 234 (2018) 90-99.

381 [32] Y. Zhu, Y. Liu, Y. Lv, Q. Ling, D. Liu, Y. Zhu, Enhancement of photocatalytic activity for BiPO<sub>4</sub>  
382 4 via phase junction, *Journal of Materials Chemistry A*, 2 (2014) 13041-13048.

383 [33] Y. Wang, Z. Qiang, W. Zhu, W. Yao, S. Tang, Z. Yang, J. Wang, J. Duan, C. Ma, R. Tan, BiPO<sub>4</sub>  
384 Nanorod/Graphene Composite Heterojunctions for Photocatalytic Degradation of Tetracycline  
385 Hydrochloride, *ACS Applied Nano Materials*, 4 (2021) 8680-8689.

386 [34] Y. Naciri, A. Hsini, Z. Ajmal, J. Navío, B. Bakiz, A. Albourine, M. Ezahri, A. Benlhachemi,  
387 Recent progress on the enhancement of photocatalytic properties of BiPO<sub>4</sub> using  $\pi$ -conjugated  
388 materials, *Advances in colloid and interface science*, 280 (2020) 102160.

389 [35] S. Kumar, P. Karfa, K.C. Majhi, R. Madhuri, Photocatalytic, fluorescent BiPO<sub>4</sub>@ Graphene  
390 oxide based magnetic molecularly imprinted polymer for detection, removal and degradation of  
391 ciprofloxacin, *Materials Science and Engineering: C*, 111 (2020) 110777.

392 [36] A.B. Azzam, R. Djellabi, S.M. Sheta, S. El-Sheikh, Ultrafast conversion of carcinogenic 4-  
393 nitrophenol into 4-aminophenol in the dark catalyzed by surface interaction on BiPO<sub>4</sub>/gC<sub>3</sub>N<sub>4</sub>  
394 nanostructures in the presence of NaBH<sub>4</sub>, RSC Advances, 11 (2021) 18797-18808.

395 [37] R. Djellabi, M. Ghorab, G. Cerrato, S. Morandi, S. Gatto, V. Oldani, A. Di Michele, C. Bianchi,  
396 Photoactive TiO<sub>2</sub>-montmorillonite composite for degradation of organic dyes in water, Journal of  
397 Photochemistry and Photobiology A: Chemistry, 295 (2014) 57-63.

398 [38] V. Nithya, B. Hanitha, S. Surendran, D. Kalpana, R.K. Selvan, Effect of pH on the sonochemical  
399 synthesis of BiPO<sub>4</sub> nanostructures and its electrochemical properties for pseudocapacitors,  
400 Ultrasonics sonochemistry, 22 (2015) 300-310.

401 [39] A. Ahmed, Y. Chaker, E.H. Belarbi, O. Abbas, J. Chotard, H. Abassi, A.N. Van Nhien, M. El  
402 Hadri, S. Bresson, XRD and ATR/FTIR investigations of various montmorillonite clays modified by  
403 monocationic and dicationic imidazolium ionic liquids, Journal of Molecular Structure, 1173 (2018)  
404 653-664.

405 [40] V.-P. Dinh, P.-T. Nguyen, M.-C. Tran, A.-T. Luu, N.Q. Hung, T.-T. Luu, H.T. Kiet, X.-T. Mai,  
406 T.-B. Luong, T.-L. Nguyen, HTDMA-modified bentonite clay for effective removal of Pb (II) from  
407 aqueous solution, Chemosphere, 286 (2022) 131766.

408 [41] P. Chand, A. Joshi, S. Saini, S. Lal, Sol-Gel Assisted Morphology and Phase Dependent  
409 Electrochemical Performance of BiPO<sub>4</sub> Nanostructures for Energy Storage Applications, Journal of  
410 Alloys and Compounds, (2021) 163315.

411 [42] X. Wang, Y. Ren, Y. Li, G. Zhang, Fabrication of 1D/2D BiPO<sub>4</sub>/g-C<sub>3</sub>N<sub>4</sub> heterostructured  
412 photocatalyst with enhanced photocatalytic efficiency for NO removal, Chemosphere, 287 (2022)  
413 132098.

414 [43] H. Ye, H. Lin, J. Cao, S. Chen, Y. Chen, Enhanced visible light photocatalytic activity and  
415 mechanism of BiPO<sub>4</sub> nanorods modified with AgI nanoparticles, Journal of Molecular Catalysis A:  
416 Chemical, 397 (2015) 85-92.

417 [44] N. Shaham-Waldmann, Y. Paz, Beyond charge separation: The effect of coupling between  
418 titanium dioxide and CNTs on the adsorption and photocatalytic reduction of Cr (VI), *Chemical*  
419 *engineering journal*, 231 (2013) 49-58.

420 [45] C. Langford, M. Izadifard, E. Radwan, G. Achari, Some observations on the development of  
421 superior photocatalytic systems for application to water purification by the “adsorb and shuttle” or  
422 the interphase charge transfer mechanisms, *Molecules*, 19 (2014) 19557-19572.

423